Title

Single-particle cryo-EM data acquisition by using direct electron detection camera

Journal

Microscopy, 65(1)

ISSN

2050-5698

Authors

Wu, Shenping

Armache, Jean-Paul

Cheng, Yifan

Publication Date

2016-02-01

DOI

10.1093/jmicro/dfv355

Peer reviewed

MICROSCOPY

Microscopy, 2016, 35–41
doi: 10.1093/jmicro/dfv355
Advance Access Publication Date: 6 November 2015

Review

Single-particle cryo-EM data acquisition by using direct electron detection camera

Shenping Wu[1], Jean-Paul Armache[1], and Yifan Cheng[1,2,*]

[1]Department of Biochemistry and Biophysics, University of California San Francisco, 600 16th Street, San Francisco, CA 94158, USA, and [2]Howard Hughes Medical Institute, University of California San Francisco, 600 16th Street, San Francisco, CA 94158, USA

*To whom correspondence should be addressed. E-mail: ycheng@ucsf.edu

Received 13 August 2015; Accepted 8 October 2015

Abstract

Recent advances in single-particle electron cryo-microscopy (cryo-EM) were largely facilitated by the application of direct electron detection cameras. These cameras feature not only a significant improvement in detective quantum efficiency but also a high frame rate that enables images to be acquired as 'movies' made of stacks of many frames. In this review, we discuss how the applications of direct electron detection cameras in cryo-EM have changed the way the data are acquired.

Key words: electron cryo-microscopy, single-particle cryo-EM, direct electron detection camera

Introduction

Single-particle electron cryo-microscopy (cryo-EM) determines three-dimensional (3D) structures of biological macromolecules from electron microscopic images of macromolecules embedded in a thin layer of vitreous ice in random orientations. Each image represents a specific projection view of the molecule along the direction of the electron beam. A 3D structure of the macromolecule is reconstructed computationally by combining many different views of the same molecule [1]. In cryo-EM, radiation damage of biological molecules by the high-energy electron beam is a major concern and predetermines how cryo-EM images are recorded in the past. To preserve high-resolution structural information, images were recorded with an extremely low total electron dose, usually below $20e^{-}$ Å^{-2} at the specimen level [2]. In comparison, total electron typically used to image inorganic specimens, such as oriented gold, is 10–100 times higher. Such low electron dose leads to an extremely low signal-to-noise ratio (SNR) in individual images. To obtain a 3D reconstruction at high resolution, it is necessary to align and average tens of thousands (or even hundreds of thousands) of individual particle images to provide different projection views of the macromolecule and more importantly to improve the SNR of the reconstruction. Many years ago, Richard Henderson analyzed the scattering power of high-energy electrons by biological macromolecules and predicted that it is possible to determine a 3D structure of an asymmetrical biological macromolecule as small as 100 kDa in molecular weight to resolutions better than 3 Å by using <10 000 projection images [3]. While this goal has not yet been accomplished fully, novel technologies and rapid progress associated with these novel technologies in recent years have moved the technique of single-particle cryo-EM closer to accomplishing this goal than ever before.

High-resolution structure determination by single-particle cryo-EM requires collecting and processing a large number of cryo-EM images of frozen hydrated samples. Assuming each electron micrograph contains ~100 particles, a complete

dataset would require hundreds or even thousands of electron micrographs. Considering that sample heterogeneity, both conformational and compositional, is inevitably present in almost every biochemically well-behaved sample, computationally sorting out a homogeneous subset of images for high-resolution 3D reconstruction would require starting with an even larger dataset. Consequently, throughput is clearly a major factor that one has to consider in collecting single-particle cryo-EM dataset. Furthermore, a high-quality image must contain sufficient signals at both high and low resolutions. The quality of the data can be evaluated based on the visibility of Thon rings in the power spectra calculated from the EM images. Structure determination aiming to achieve high resolution requires images that give Thon rings extending to high resolution. At the same time, the low-resolution signal that contributes to image contrast is important for particle picking and image processing. In this review, we focus our discussions on how technological breakthroughs in cameras influence the ways that single-particle cryo-EM data are acquired.

Image acquisition prior to direct electron detection

Traditionally, electron micrographs of frozen hydrated biological molecules were recorded with either photographic film or scintillator-based digital cameras, such as charge-coupled device (CCD) or complementary metal-oxide semiconductor (CMOS) cameras. In general, photographic film provides a better detective quantum efficiency (DQE, a measure of camera performance as a function of spatial frequency) at high frequency than scintillator-based cameras [4,5]. It also has a larger size than all digital cameras. After digitization using a scanner with 7 μm step size, a 10 cm × 8 cm photographic film becomes a digital image of ~12 k × 10 k pixels. In comparison, the sensors of most digital cameras only have 4 k × 4 k or fewer pixels, except a handful that have 8 k × 8 k pixels. Thus, film was often the preferred medium to record cryo-EM images for high-resolution structure determination, both for single-particle cryo-EM and electron crystallography experiments [6,7]. When using photographic film for high-resolution cryo-EM image acquisition, a user needs to consider matching the magnification of the microscope with the scanner step size so that the targeted resolution corresponds to about half of the Nyquist frequency. The beam intensity should be optimized to have an exposure time preferably <1 s (so that sample motion-induced deterioration of image quality can be minimized) and film optical density close to 1. Defocus needs to be set high enough to produce sufficient image contrast for particle visualization. The contrast of cryo-EM images recorded using photographic films is often poor because film has a poor DQE at low frequency, forcing images to be recorded with relative high defocii [8]. Film does not have the capability of providing immediate feedback, thus preventing automated data acquisition. It requires chemical development and fixation, followed by extensive washing and drying, before it can be digitized using a high-quality scanner. This tedious process greatly limits the throughput of single-particle cryo-EM and electron crystallography.

Compared with film, scintillator-based digital cameras, either CCD or CMOS, have the benefit of providing digital images immediately after exposure, which greatly facilitated the implementation of automated image acquisitions [9]. These cameras use a thin layer of phosphor scintillator to convert signals from incident electrons to photons that are then recorded by the cameras. They typically have a poorer high-frequency DQE but a better low-frequency DQE than film [4,5]. Thus, images recorded using cameras with scintillator often have better contrast than photographic film recorded under the same condition. Concerning the poor high-frequency DQE, images are usually recorded at a higher magnification to take advantage of better DQE at low frequency. Higher magnification, however, reduces the total number of particles captured in a single micrograph. Thus, collecting images with either film or scintillator-based CCD/CMOS camera would require optimizing the imaging conditions accordingly.

Image acquisition using direct electron detection cameras

The wide application of direct electron detection device (DDD) cameras enabled a 'resolution revolution' in single-particle cryo-EM [10]. All DDD cameras have significantly higher DQEs than photographic film and scintillator-based cameras [4,5,11]. The high frame rate of DDD cameras enables the recording of cryo-EM data as dose-fractionated image stacks instead of as a single micrograph [12]. Collection of image stacks enables correction of stage- or beam-induced motion and significantly improves image quality by recovering the high-resolution signal deteriorated by that motion [4,13,14]. Furthermore, it provides an effective way to deal with rapid radiation damage, allowing images to be recorded with a significantly higher total electron dose because high-resolution noise from the later frames may be removed or down-weighted at a later stage of image processing [4,15]. This approach boosts image contrast and, at the same time, excludes high-frequency noise caused by radiation damage from the final reconstruction. Together, these novel features of DDD enable routine near-atomic structure determination of

biological macromolecules, from large assemblies to small integral membrane proteins.

DDD cameras operated in integration mode record electron micrographs by integrating charges generated by high-energy electrons striking the camera sensor. Without a phosphor scintillator to convert the primary electron signal to light signal, charges generated by a single primary electron event distribute over a small region with a much smaller point-spread function (PSF), which leads to a significantly improved DQE. All commercial DDD cameras (Falcon camera from FEI Company, DE camera from Direct Electron and K2 camera from Gatan, Inc.) can operate in this way. In addition to integration mode, the K2 Summit records electron micrographs by counting individual primary electron events and centroiding the event to an area that is a quarter of the pixel. It achieves single electron counting by using a high internal frame rate of 400 frames per second (fps) so that in each frame the individual primary electron events can be identified and counted. Counting primary electron events not only reduces the PSF to a single pixel, but it also removes the Landau noise as well as readout noise, which is inevitable in regular charge integration mode. Single electron counting greatly improves the DQE, particularly, at low resolution [4]. Centroiding quadruples the total number of pixel in an image and extends the Nyquist limit to twice of the Nyquist limit defined by the physical pixel size. The drawback of a counting camera is that it requires a relatively low electron dose rate on the camera to minimize the effect of coincidence loss, i.e., when two primary electron events overlap, only one event is counted and the other is lost, which causes certain image artifacts [16].

DDD cameras have unique properties in comparison with films and scintillator-based cameras. They have completely changed the way how cryo-EM images are acquired. To take full advantage of DDD cameras, it is necessary to optimize the data acquisition strategy based on the type of the camera used. For the K2 Summit operating in counting mode, it is important to optimize the dose rate on the camera. Typically, images are recorded at a dose rate of $10e^{-}$ pixel^{-1} s^{-1} [4,17] or less [18]. Using lower dose rate can improve DQE, but at the expense of a longer exposure time to accumulate the same total dose, which may lead to larger file sizes. In addition, when images are recorded using the same number of frames per second, lower dose rate results in lower SNR per frame, making it harder for motion correction. However, these drawbacks could be overcome by more robust algorithms for motion correction and better methods of data compression and storage.

Despite all of the benefits discussed above, users of DDDs may face new challenges due to the unique design of these devices. One of them is the smaller pixel size compared with common CCD cameras. The size of a pixel of a CCD camera is typically around 15 μm. When working with CCD cameras installed on FEI microscopes without energy filters, the typical nominal magnification that gives a pixel size of 1 Å at the specimen level is around 100 000×. In this magnification range, projection lenses are well tuned to minimize distortions. Among the three series of DDDs, the FEI Falcon has a pixel size of 14 μm, thus allowing users to work at similar nominal magnifications as they do with CCD cameras. However, the Gatan K2 series and Direct Electron DE series have pixel sizes between 5 and 6.5 μm and thus require users to use a significantly lower magnification in order to achieve a comparable pixel size at the specimen level [4]. There are multiple reports of observation of anisotropic magnification on FEI microscopes equipped with K2 cameras [19] with the distortion of usually a few percent. This problem needs to be resolved by manufacturers by improving microscope performance at lower magnifications. It is also possible to compensate for the distortion by post-processing. A small amount of anisotropic magnification may not have a big effect on small proteins, but it can be very detrimental to large complexes, such as a ribosome or a virus. There are multiple ways to correct the distortion [19,20], including real space stretching using bilinear interpolation and the Fourier space interpolation [15,21].

In addition to anisotropic magnification, low nominal magnification poses another potential problem for early generations of FEI microscopes without constant power lenses. At certain magnifications near 30 000×, the intermediate lens is nearly switched off, causing a measurable reduction in image quality. The influence of this effect on the final results has yet to be well characterized. It may also depend on individual microscopes.

Processing image stacks

It is possible to obtain a high-resolution structure without collecting images as stacks and correcting sample motions captured during the exposure [22]. There are various experimental approaches aimed at reducing beam-induced image motion, such as using spots-scan imaging technique [23], a thick continuous carbon layer to support the sample [24], using gold grids [25] or using special objective aperture [26]. However, all these methods reduce but do not completely eliminate image motion, either from charge-induced image motion or thermal-instability-induced sample motion. Collecting cryo-EM data as image stacks and correcting motion computationally may improve image quality, if done properly.

All three types of commercial DDD cameras are capable of recording cryo-EM images as image stacks with output

frame rates ranging from 18 to 40 fps. When using integration mode, the typical exposure time is relatively short, around 1 s. These 'movies' contain mostly charge-induced motion [13]. For K2 Summit operating in counting mode, coincidence loss is a major concern, and the optimal total exposure time is significantly longer. Motion captured in these 'movie' stacks is a combination of charge-induced motion and long-range sample drift [4]. Without correction, this image motion could severely deteriorate image quality.

Various tools are now available to correct image motion recorded in 'movie' stacks, such as Motioncorr [4], movie processing in RELION [13,27], optical flow [28] and alignparts lmbfgs [29]. Furthermore, tools that are used to align tilt series from tomographic data can be repurposed to align movie frames of single-particle data recorded with DDDs [18]. Each tool has its unique approach and features that are specifically designed to deal with either global or local motion (such as correcting motion per particle). Images recorded with the K2 Summit usually contain some global motions, due to the relative long exposure time being used, in contrast to images recorded using integration mode, with typically less global motion. Thus, depending on how cryo-EM images are recorded, one motion correction algorithm may work better than the other, and it may be necessary to combine different algorithms.

In addition to correcting image motion, recording a cryo-EM image as a 'movie' stack also provides means to deal with radiation damage. Nowadays, cryo-EM images

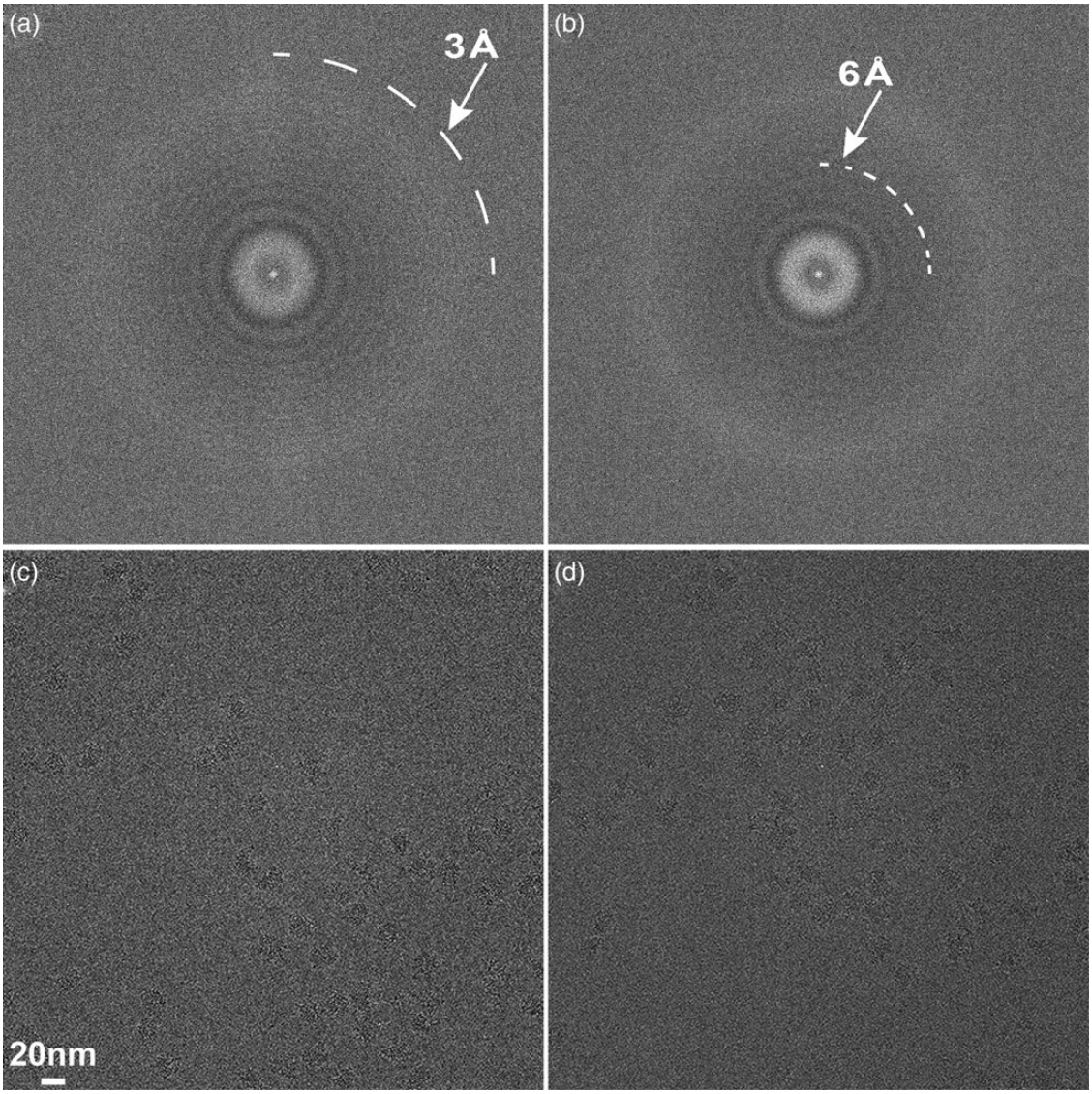

Fig. 1. Comparison of images recorded from different ice thicknesses. Images of frozen hydrated ribosome particles without a supporting carbon film were recorded from different areas of the same grid. FFT (a) of an image from thin ice (c) has visible Thon rings at ~3 Å resolution. FFT (b) of an image from thick ice (d) has fewer Thon rings.

are routinely recorded using a significantly higher total dose on the specimen than what was typically used prior to the 'DDD era' (~20e^- Å^{-2}). One can select different ranges of frames for different purposes. For example, after image motion correction, a simple average of the entire stack usually has strong image contrast, essential for particle picking and facilitating accurate particle alignment. After obtaining a good alignment, the user may discard the first few frames, which usually suffer a large uncorrectable motion, and the later ones that suffer significant radiation damage and only use frames that have well-preserved high-resolution signals to calculate the final reconstruction [4,17,18]. Instead of discarding the frames that are deteriorated by motion or radiation damage, a better approach is to apply a low-pass filter to each frame, down-weighting compromised high-resolution signal in frames before averaging them. Such frame weighting strategies are implemented in a number of software packages [15,27].

Potential limitations and possible approaches to overcome

A number of reviews or studies have discussed possible factors that may limit the resolution of single-particle reconstruction [30]. Sample heterogeneity is clearly a major factor that influences the achievable resolution. This situation can be improved either biochemically or computationally. In addition, there are many other experimental factors that may limit image quality and ultimately limit the final resolution of a 3D reconstruction. Current motion correction algorithms are still not perfect, and there is also un-correctable motion that is captured in a single frame (especially, in the first few frames). High-frequency acoustic noise could induce sample vibration that cannot be corrected computationally. Imperfect illumination and optical aberrations could cause geometric distortions in images. Furthermore, ice thickness has a strong influence on the final achievable resolution of single-particle reconstruction. Images recorded from thin ice often show visible Thon rings at a higher resolution than that of images recorded from thicker ice (Fig. 1). When a molecule is embedded in a layer of vitreous ice that is much thicker than the diameter of the molecule, particles are distributed at different z-position along the direction of the electron beam. As fitting Thon rings to the calculated power spectrum of a micrograph only gives the average defocus values, each particle in the micrograph has an error in defocus associated with their individual z-positions. Averaging particles with defocii distributed over a range due to the ice thickness causes deterioration of the high-resolution structural information (Fig. 2).

Ideally, ice should be as thin as possible to still accommodate the particle of interest. Careful selection of images taken from holes with the thinnest possible ice helps to improve the Thon ring visibility at high frequencies, as well as the resolution of the final 3D reconstruction [18]. However, this is not a generally applicable approach. Making

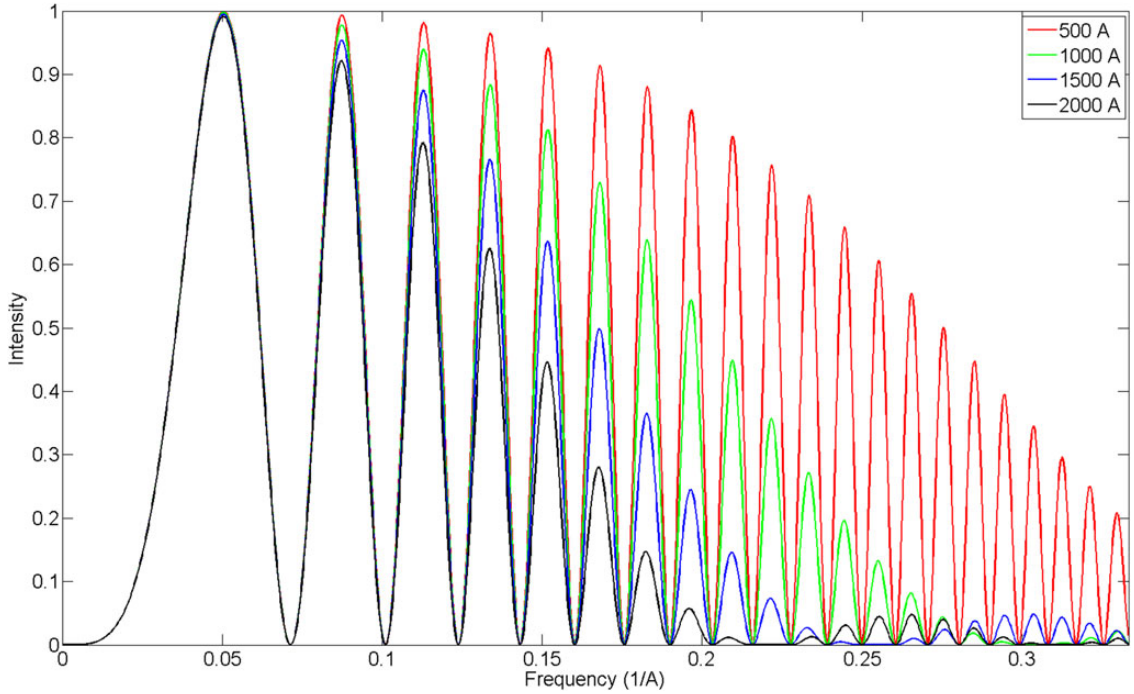

Fig. 2. Influence of ice thickness on CTF. With the average defocus set to −1 μm, the CTF were averaged over different ice thickness: 500 Å (red), 1000 Å (green), 1500 (light blue) and 2000 Å (dark blue). The envelope of the CTF drops significantly with increasing ice thickness.

cryo-EM grids with thin ice is not always possible, as particles are often only distributed in areas where ice is much thicker than the size of the particle. Integral membrane proteins solubilized in detergent often behave in this way [31]. An ultimate solution would be to determine (or refine) defocus values for individual particles within the same micrograph. However, current structure refinement procedures cannot produce reliable and accurate defocus value for individual particles. Because low-resolution image information is not as sensitive to Contrast Transfer Function (CTF) modulation as high-resolution information, accurate CTF determination would require including noisy high-resolution information into the refinement. However, including high-resolution information during refinement may lead to model-induced bias, which is a major concern in all image-processing strategies. An alternative solution to circumvent the problem is to record images with low defocii. These images have fewer CTF oscillations beyond the first zero, and CTF correction can tolerate more defocus error. However, the caveat is that low contrast may make motion corrections harder. If robust phase plates become available, cryo-EM images could be collected at close to the Scherzer focus. Since there would be no CTF correction within the first CTF zero, images would be insensitive to certain level of defocus error.

Conclusion

For many years, it has been known that a modern electron microscope equipped with a field emission gun (FEG) electron source has the capability of delivering images of an inorganic material specimen at atomic resolution [32]. Traditional methods of collecting cryo-EM images had to deal with two major technical limitations. One is the radiation damage that limits the total dose that can be used to image biological molecules and results in noisy images. The other is beam-induced image motion, which deteriorates high-resolution signals captured in images. It was difficult to circumvent these two limiting factors by using traditional methods with photographic film or scintillator-based digital cameras. DDD-based movie technology enabled us to overcome these limiting factors and enabled single-particle cryo-EM to achieve near-atomic resolution structure determination rather quickly and routinely. By optimizing imaging conditions according to specific characteristics of the camera being used, it is possible to push cryo-EM technology further to achieve higher resolutions from a broader range of biological molecules.

Funding

This work was supported by the Howard Hughes Medical Institute and grants from National Institutes of Health grants R01GM082893, R01GM098672, P50GM082250 and P01GM111126. Y.C. is an investigator with the Howard Hughes Medical Institute.

References

1. Cheng Y, Grigorieff N, Penczek P A, Walz T (2015) A primer to single-particle cryo-electron microscopy. *Cell* 161: 438–449.
2. Stark H, Zemlin F, Boettcher C (1996) Electron radiation damage to protein crystals of bacteriorhodopsin at different temperatures. *Ultramicroscopy* 63: 75–79.
3. Henderson R (1995) The potential and limitations of neutrons, electrons and X-rays for atomic resolution microscopy of unstained biological molecules. *Q Rev Biophys*. 28: 171–193.
4. Li X, Mooney P, Zheng S, Booth C R, Braunfeld M B, Gubbens S, Agard D A, Cheng Y (2013) Electron counting and beam-induced motion correction enable near-atomic-resolution single-particle cryo-EM. *Nature Methods* 10: 584–590.
5. McMullan G, Faruqi A R, Clare D, Henderson R (2014) Comparison of optimal performance at 300 keV of three direct electron detectors for use in low dose electron microscopy. *Ultramicroscopy* 147: 156–163.
6. Murata K, Mitsuoka K, Hirai T, Walz T, Agre P, Heymann J B, Engel A, Fujiyoshi Y (2000) Structural determinants of water permeation through aquaporin-1. *Nature* 407: 599–605.
7. Zhang X, Jin L, Fang Q, Hui W H, Zhou Z H (2010) 3.3 A cryo-EM structure of a nonenveloped virus reveals a priming mechanism for cell entry. *Cell* 141: 472–482.
8. Cheng Y (2015) Single-particle cryo-EM at crystallographic resolution. *Cell* 161: 450–457.
9. Suloway C, Pulokas J, Fellmann D, Cheng A, Guerra F, Quispe J, Stagg S, Potter C S, Carragher B (2005) Automated molecular microscopy: the new Leginon system. *J. Struct. Biol.* 151: 41–60.
10. Kuhlbrandt W (2014) Biochemistry. The resolution revolution. *Science* 343: 1443–1444.
11. Ruskin R S, Yu Z, Grigorieff N (2013) Quantitative characterization of electron detectors for transmission electron microscopy. *J. Struct. Biol.* 184: 385–393.
12. Brilot A F, Chen J Z, Cheng A, Pan J, Harrison S C, Potter C S, Carragher B, Henderson R, Grigorieff N (2012) Beam-induced motion of vitrified specimen on holey carbon film. *J. Struct. Biol.* 177: 630–637.
13. Bai X C, Fernandez I S, McMullan G, Scheres S H (2013) Ribosome structures to near-atomic resolution from thirty thousand cryo-EM particles. *eLife* 2: e00461.
14. Campbell M G, Cheng A, Brilot A F, Moeller A, Lyumkis D, Veesler D, Pan J, Harrison S C, Potter C S, Carragher B, Grigorieff N (2012) Movies of ice-embedded particles enhance resolution in electron cryo-microscopy. *Structure* 20: 1823–1828.
15. Grant T, Grigorieff N (2015) Measuring the optimal exposure for single particle cryo-EM using a 2.6 A reconstruction of rotavirus VP6. *eLife* 4: e06980.
16. Li X, Zheng S Q, Egami K, Agard D A, Cheng Y (2013) Influence of electron dose rate on electron counting images recorded with the K2 camera. *J. Struct. Biol.* 184: 251–260.
17. Liao M, Cao E, Julius D, Cheng Y (2013) Structure of the TRPV1 ion channel determined by electron cryo-microscopy. *Nature* 504: 107–112.

18. Bartesaghi A, Merk A, Banerjee S, Matthies D, Wu X, Milne J L, Subramaniam S (2015) Electron microscopy. 2.2 A resolution cryo-EM structure of beta-galactosidase in complex with a cell-permeant inhibitor. *Science* 348: 1147–1151.
19. Zhao J, Brubaker M A, Benlekbir S, Rubinstein J L (2015) Description and comparison of algorithms for correcting anisotropic magnification in cryo-EM images. *J. Struct. Biol.* doi: 10.1016/j.jsb.2015.06.014.
20. Grant T, Grigorieff N (2015) Automatic estimation and correction of anisotropic magnification distortion in electron microscopes. *J. Struct. Biol.* doi: 10.1016/j.jsb.2015.08.006.
21. Zhao J, Benlekbir S, Rubinstein J L (2015) Electron cryomicroscopy observation of rotational states in a eukaryotic V-ATPase. *Nature* 521: 241–245.
22. Fischer N, Neumann P, Konevega A L, Bock L V, Ficner R, Rodnina M V, Stark H (2015) Structure of the *E. coli* ribosome-EF-Tu complex at <3 A resolution by Cs-corrected cryo-EM. *Nature* 520: 567–570.
23. Zhou Z H, Prasad B V, Jakana J, Rixon F J, Chiu W (1994) Protein subunit structures in the herpes simplex virus A-capsid determined from 400 kV spot-scan electron cryomicroscopy. *J. Mol. Biol.* 242: 456–469.
24. Glaeser R M, Downing K H (2004) Specimen charging on thin films with one conducting layer: discussion of physical principles. *Microsc. Microanal.* 10: 790–796.
25. Russo C J, Passmore L A (2014) Electron microscopy: ultrastable gold substrates for electron cryomicroscopy. *Science* 346: 1377–1380.
26. Berriman J A, Rosenthal P B (2012) Paraxial charge compensator for electron cryomicroscopy. *Ultramicroscopy* 116: 106–114.
27. Scheres S H (2014) Beam-induced motion correction for sub-megadalton cryo-EM particles. *eLife* 3: e03665.
28. Abrishami V, Vargas J, Li X, Cheng Y, Marabini R, Sorzano C O, Carazo J M (2015) Alignment of direct detection device micrographs using a robust optical flow approach. *J. Struct. Biol.* 189: 163–176.
29. Rubinstein J L, Brubaker M A (2015) Alignment of cryo-EM movies of individual particles by optimization of image translocations. *arXiv* arXiv:1409.6789v2.
30. Agard D A, Cheng Y, Glaeser R M, Subramaniam S (2014) Single-particle cryo-electron microscopy (cryo-EM): progress, challenges, and perspectives for future improvement. *Adv Imag Electr Phys* 185: 113–137.
31. Kim J, Wu S, Tomasiak T, Mergel C M, Winter M B, Stiller S B, Robles-Colmanares Y, Stroud R M, Tampe R, Craik C S, Cheng Y (2014) Subnanometer resolution cryo-EM structure of a nucleotide free heterodimeric ABC exporter. *Nature* 517: 396–400.
32. Azubel M, Koivisto J, Malola S, Bushnell D, Hura G L, Koh A L, Tsunoyama H, Tsukuda T, Pettersson M, Hakkinen H, Kornberg R D (2014) Nanoparticle imaging. Electron microscopy of gold nanoparticles at atomic resolution. *Science* 345: 909–912.